ACS Macro Letters

Letter

pubs.acs.org/macroletters

Molecular Design of Liquid Crystalline Brush-Like Block Copolymers for Magnetic Field Directed Self-Assembly: A Platform for Functional Materials

Prashant Deshmukh,[†,#] Manesh Gopinadhan,[§,#] Youngwoo Choo,[§] Suk-kyun Ahn,[‡,⊥] Pawel W. Majewski,[§] Sook Young Yoon,[†] Olgica Bakajin,[∥] Menachem Elimelech,[§] Chinedum O. Osuji,[§] and Rajeswari M. Kasi*[,†,‡]

[†]Department of Chemistry, University of Connecticut, Storrs, Connecticut 06269, United States

[‡]Polymer Program, Institute of Material Science, University of Connecticut, Storrs, Connecticut 06269, United States

[§]Department of Chemical and Environmental Engineering, Yale University, New Haven, Connecticut 06511, United States

[∥]Porifera Nano Inc., Hayward, California 94545, United States

Supporting Information

ABSTRACT: We report on the development of a liquid crystalline block copolymer with brush-type architecture as a platform for creating functional materials by magnetic-field-directed self-assembly. Ring-opening metathesis of *n*-alkyloxy cyanobiphenyl and polylactide (PLA) functionalized norbornene monomers provides efficient polymerization yielding low polydispersity block copolymers. The mesogenic species, spacer length, monomer functionality, brush-chain length, and overall molecular weight were chosen and optimized to produce hexagonally packed cylindrical PLA domains which self-assemble and align parallel to an applied magnetic field. The PLA domains can be selectively removed by hydrolytic degradation resulting in the production of nanoporous films. The polymers described here provide a versatile platform for scalable fabrication of aligned nanoporous materials and other functional materials based on such templates.

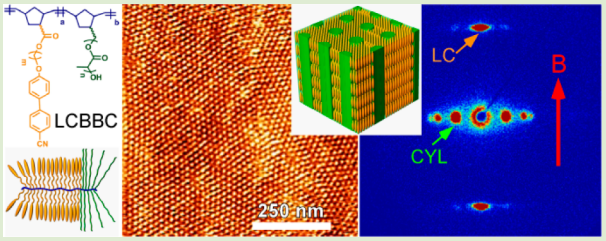

Self-assembly of block copolymers (BCPs) provides a variety of nanostructured morphologies for use in surface patterning, as membranes for lithium ion conduction in batteries, water purification, or analytical separations, and in the creation of nanostructured electro-optical materials for photovoltaics and photonics.[1,2] The ability to control the orientation of these self-assembled structures over the length scale of interest is critical to harnessing the utility of BCPs in the aforementioned areas. Control of orientation may be achieved using electric fields and shear fields, but this remains a challenging proposition in terms of scalability and stability of the polymer matrix. For example, nanoporous membranes may be attained by BCP alignment using electric fields,[3] shear alignment,[4] solvent treatment,[5,6] blending homopolymers or ligands,[7−9] and surface modification.[10] All aforementioned techniques are system specific and oftentimes very sensitive to external conditions; moreover, orientation extends only few periodicities in the through thickness direction. More importantly, the vertical or perpendicular alignment of cylindrical microdomains in thin films using scalable methods is especially difficult to achieve,[11] and it is this geometry which is most often required for the applications discussed. Magnetic fields offer significant promise in this regard due to their space pervasive nature and their inherent scalability as well as use of a noncontact method of field application.[4] Their utilization however relies on the presence of suitable magnetic anisotropy and a confluence of other characteristics that are seldom encountered in typical BCPs. There is thus a strong need for BCPs which are deliberately engineered for magnetic field directed self-assembly (DSA) as a route to the creation of functional materials, as schematically shown in Figure 1 and, moreover, for the development of structure−property relationships which make such molecular engineering possible.

The need for magnetic anisotropy ($\Delta\chi$) in the BCP can be satisfied by the incorporation of a rigid anisotropic moiety such as a biphenyl mesogen either directly in the polymer backbone or as a side chain.[12] The self-assembly of these mesogens into a liquid crystalline mesophase provides the handle for magnetic field control of the BCP superstructure. The orientation of the mesogen with respect to the interface between the blocks and the sign of its $\Delta\chi$ combine to dictate the alignment of the BCP domains under application of a magnetic field.[12,13] In this case, the desire is to use a mesogen with a positive anisotropy that assumes a planar anchoring condition at the cylindrical block interface. This results in parallel alignment of cylindrical microdomains under the field.

Received: March 17, 2014
Accepted: April 28, 2014
Published: May 1, 2014

   dx.doi.org/10.1021/mz500161k | *ACS Macro Lett.* 2014, 3, 462−466

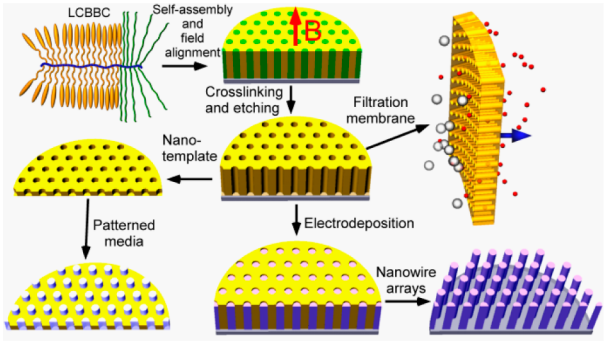

Figure 1. In this report we introduce a novel cylinder-forming liquid crystalline brush-type BCP architecture (LCBBC) suitable for magnetic field DSA for the scalable fabrication of nanoporous monoliths with no thickness constraints. The resulting nanoporous membranes by field alignment and selective removal of the cylindrical block composed of polylactide (PLA) chains can potentially serve as a platform for the design of functional materials.

Magnetic field DSA can be implemented by simply cooling the sample across its highest temperature liquid crystal transition, T_D, while in the presence of the field. The formation of the liquid crystal (LC) mesophase within the BCP superstructure during the cooling provides the driving force for alignment. The alignment kinetics are dictated by the viscosity of the system. This in turn depends strongly on the state of order of the BCP superstructure as determined by the proximity to the order−disorder transition temperature, T_{ODT}. A large separation of the two temperatures with $T_{ODT} > T_I$ results in sluggish alignment as the system is in a high viscosity microdomain-ordered state prior to crossing T_I.

Ideally T_{ODT} should be coincident with T_I as this situation maximizes the coupling of the rapidly increasing magnetic driving force for alignment with the rapidly decreasing mobility as the system is cooled across concurrent ordering transitions.[14] This can be accomplished by designing a weakly segregated system in which ordering of the BCP superstructure is explicitly driven by the smaller length scale LC self-assembly. The alignment kinetics may also be enhanced through the use of chain architectures which have a decreased propensity for entanglement at a given molecular weight. Brush architectures exhibit this characteristic due to the extended nature of the polymer backbone driven by side-chain crowding.[15,16] Thus, a departure from linear chain architectures may be expected to confer some benefit. While the use of low viscosity materials improves alignment kinetics, the stability of nanopores produced in a soft material would be quite limited due to the effects of Laplace pressure.[17,18] The system should therefore be made mechanically robust enough to resist pore collapse before the nanopores are generated.[19,20] A natural way to do this is to cross-link the polymer, and so the use of an unsaturated or otherwise reactive BCP backbone is desirable. Finally, the nanopores themselves would be produced by selective degradation of the minority component of the BCP.

Here we demonstrate de novo design and synthesis of a LC BCP that displays the above-discussed characteristics for field alignment of cylindrical microdomains. The blocks present contrasting polarity, with the ability to selectively remove the minority domains and to cross-link the continuous matrix for future use. It thus provides a versatile platform which can be used to create aligned selective transport membranes over macroscopic areas and thicknesses or to produce nanoporous films which themselves can serve as templates for functional materials produced by templated synthesis and/or pattern transfer as shown in Figure 1. The structure of the BCP is shown in Figure 2. We employ a brush-like architecture using a

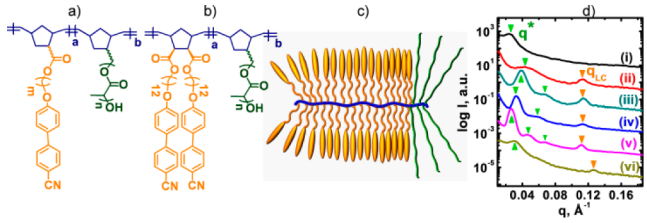

Figure 2. Schematic of LCBBC: (a) monosubstituted mesogen, (b) disubstituted mesogen, where methylene spacers (m) are 6 or 12 and M_w of PLA side chain is 1, 2, or 3 kDa. (c) Illustration of LCBBC architecture. (d) SAXS data demonstrating the effect of side-chain length of PLA on self-assembled hierarchical structure in LCBBC: (i) $(NBCB6)_{50}$-*b*-$(NBPLA3k)_2$ (LC6PLA3k), (ii) $(NBCB12)_{24}$-*b*-$(NBPLA1k)_2$ (LC12PLA1k), (iii) $(NBCB12)_{22}$-*b*-$(NBPLA2k)_2$ (LC12PLA2k), (iv) $(NBCB12)_{31}$-*b*-$(NBPLA2k)_3$ (LC12PLA2k-2), (v) $(NBCB12)_{40}$-*b*-$(NBPLA3k)_{2.5}$ (LC12PLA3k), and (vi) $[NB(CB12)2]_{21}$-*b*-$(NBPLA2k)_3$ (2LC12PLA2k), where sample labels used in the manuscript are given in the brackets and q^* (green) and q_{LC} (dark yellow) arrows represent microphase segregated and smectic LC layer scattering peaks, respectively.

poly(norbornene) backbone. The majority block is side-functionalized by a cyanobiphenyl (CB) mesogen using an *n*-alkyl spacer, while the minority block is composed of poly(D,L-lactide) (PLA) side chains. In all cases asymmetric compositions with ∼75% of LC content were chosen to target the formation of hexagonally packed PLA cylinders. Nanopore generation by selective removal of the minority phase using UV degradation, ozonolysis, and chemical treatments documented in the literature is typically inadequate due to harsh etching conditions.[21−23] However, introduction of a group that can be etched under mild conditions[24] or a photocleavable junction[25] is often preferred, leaving behind the matrix material unaltered. The PLA can be selectively removed by hydrolysis under mild basic conditions,[4,24] while the CB species provides a positive $\Delta\chi$ and an expected planar anchoring at the block interface.[26,27] The norbornene (NB) backbone can be cross-linked using thiol−ene chemistry[28] to provide the required rigidity to support nanopores. Table S1 (Supporting Information) provides details of different materials that were prepared to assess the role of PLA side-chain length, alkyl spacer length, and overall molecular weight on the system. The nomenclature $(NBCBm)_a$-*b*-$(NBPLAyk)_b$ reflects the alkyl spacer length m, the degree of polymerization a of the cyanobiphenyl norbornene ($NBCBm$), the molecular weight y kg/mol of the PLA side chain, and the degree of polymerization b of the norbornenyl-PLA (NBPLA). For example, $[NB(CB12)_2]$ refers to the disubstituted NB monomer shown in Figure 2b. The details of the synthesis of the norbornenyl end-functionalized monomers and ring-opening metathesis polymerization (ROMP) of the BCPs are provided in the Supporting Information.

DSC data (Table S1 and Figure S4, Supporting Information) show the presence of a glass transition for the NB backbone (T_g ∼ 20−45 °C) and a LC clearing transition (T_I ∼ 70−85 °C) for all the polymers. We used small-angle X-ray scattering (SAXS) to examine the self-assembled structures presented by the polymers at room temperature, and data are shown in Figure

dx.doi.org/10.1021/mz500161k | ACS Macro Lett. 2014, 3, 462−466

2d. The 6-spacer material with 3k PLA side chains, LC6PLA3k, exhibits only 1 peak in SAXS, suggesting a poorly ordered morphology and no indication of smectic layering of the CB mesogens. The absence of smectic order suggests that the spacer is too short to permit sufficient motional decoupling of the mesogen from the polymer backbone as required for smectic mesophase formation.[29−31] The system does however show nematic order similar to that observed in the LC homopolymer by wide-angle measurements (Figure S5, Supporting Information). By contrast, all samples with 12-methylene spacers do show smectic LC order, with layer spacings ranging from 5.0 to 5.6 nm. Disubstitution of the NB backbone, 2LC12PLA2k, resulted in a poorly ordered material that shows only one peak in the SAXS. By contrast, a monosubstituted variant with the same PLA side chain length and overall molecular weight, LC12PLA2k, shows two peaks for BCP domains, indicating better long-range order of the self-assembled morphology. The d-spacing is d_{BCP} = 16.3 nm which corresponds to an intercylinder spacing of d_{CYL} = 18.8 nm ($d_{CYL} = (4/3)^{1/2} * d_{BCP}$). The LC layer period is 5.5 nm.

Variation of the PLA side chain length resulted in systematic differences in the degree of order exhibited by the BCPs. 1k PLA side chains in LC12PLA1k resulted in a poorly ordered system that displayed a single broad peak from the BCP with a d-spacing of 14.5 nm. The sample with 3k PLA side chains (LC12PLA3k) however produced much better order, with three nonsmectic peaks visible in the SAXS and a d-spacing of 23.6 nm. The ratios of the square of the scattering wavevectors at which the peaks were located of 1:3:4 and 1:3 for PLA3k and PLA2k side chain length BCPs indicate that they form hexagonally packed cylinders. The improvement in long-range order of the system morphology on changing the PLA side chain length from 1k to 3k cannot be decoupled at this stage from the effect of overall molecular weight as it was not possible to control the degree of polymerization precisely enough while varying the side-chain length to maintain an overall constant molecular weight. Intriguingly, the d-spacing for BCPs with 2k and 3k PLA side chains increases quite rapidly with molecular weight, with $d \sim M_w^{0.75}$. For weakly segregated linear diblocks, d-spacing scales as $M_W^{0.5}$, whereas for brush-block copolymers in the strongly stretched regime, $d \sim M_w^{1.0}$.[32] These data suggest that the system displays significant brush-like character despite the limited length of the LC side chains and that the brush-type architecture plays a strong role in the self-assembly. Overall we can conclude that monosubstitution as opposed to disubstitution and the use of a 12-spacer unit rather than a 6-spacer unit result in well-ordered materials that exhibit hexagonally packed cylinders of PLA in a smectic mesophase matrix.

Mesophase and BCP nanostructure evolution is further studied using temperature-resolved SAXS analysis. From the temperature-resolved SAXS of LC12PLA2k, Figure 3a, we extract $T_{ODT} \sim 160$ °C based on the disappearance of the second-order BCP peak. This temperature is well above $T_I \sim 75$ °C and thus represents an undesirable situation for field alignment as previously discussed. We explored the use of mesogen blending as a means of tuning the T_{ODT} of the system. 4′-(Hexyloxy)-4-biphenylcarbonitrile (CB6) was added to LC12PLA2k at a 1:1 stoichiometric ratio (R) of CB6 to NBCB12 monomer units. These free mesogens coassemble with the polymer-attached CB species and act to plasticize the system. The temperature-resolved measurements of these mesogen-blended materials show that the approach is effective

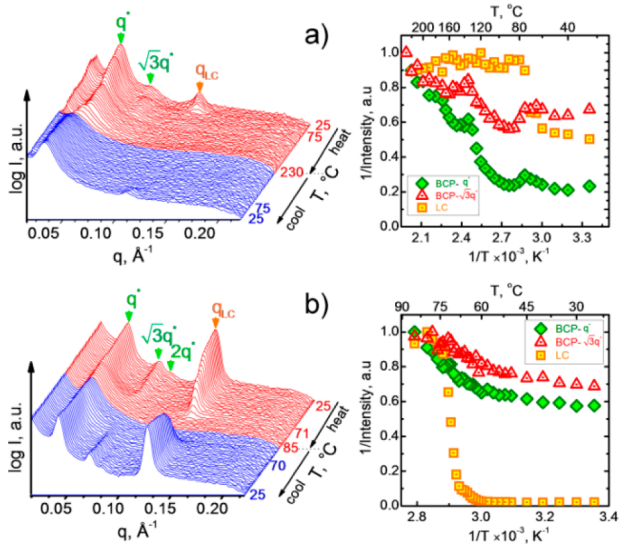

Figure 3. Temperature-resolved SAXS experiments from (a) LC12PLA2K and (b) LC12PLA2K blended with 4′-(hexyloxy)-4-biphenylcarbonitrile (CB6) at a stoichiometry of R = 1. The corresponding inverse intensities are also given (right side).

(Figure 3b). Blending results in a reduction of T_{ODT} to ∼72 °C for both LC12PLA2k and LC12PLA2k-2 (Figure S6, Supporting Information). Importantly, T_I is largely unaffected at ∼75 °C, and thus the two ordering transitions are effectively coincident, as originally desired. The d-spacing of the stoichiometric blend sample of LC12PLA2k decreased to d_{BCP} = 15.3 nm (d_{CYL} = 17.7 nm). A similar reduction in d-spacing was observed for higher M_w materials, LC12PLA2k-2 from 19.3 to 17.6 nm after mesogen blending. This is consistent with a decrease in the effective interaction parameter between the blocks as reflected by the decrease in T_{ODT}. Additionally, the LC layer periodicity decreased from 5.6 to 5 nm.

The SAXS results are confirmed by atomic force microscopy (AFM) images of the samples (thickness ∼ 100 nm) (Figure 4

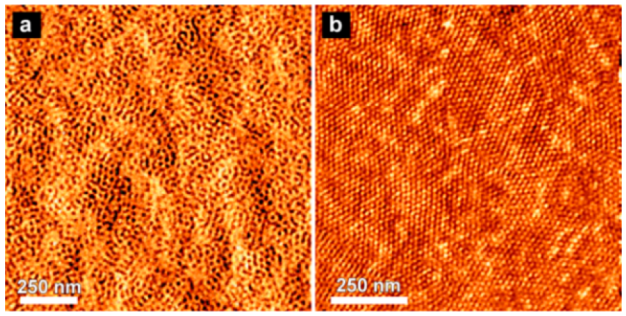

Figure 4. AFM data of LCBBC materials indicating cylindrical morphology: (a) LC12PLA2k-2 (phase image) and (b) height image of LC12PLA2k-2 blended with CB6 mesogens at R = 1.

and Figure S7, Supporting Information). LC12PLA2k shows poorly ordered cylindrical domains with diameters of ca. 7.5 nm, while for LC12PLA2k-2 the domains have diameters of ca. 12.5 nm and display slightly improved positional order. These dimensions are altered relative to those expected on the basis of the SAXS d-spacings, and estimated volume fractions, 10.3 and 12.4 nm, respectively, likely originate from the convolution of the finite tip diameter with the small feature sizes of the sample. AFM data also confirm that the CB6 blended materials form

dx.doi.org/10.1021/mz500161k | ACS Macro Lett. 2014, 3, 462−466

hexagonally ordered cylindrical domains with diameters of ca. 11.6 and 7.1 nm for LC12PLA2k-2 and LC12PLA2k, respectively.

For the magnetic field alignment, samples of LC12PLA2k and LC12PLA2k-2 were cooled from 220 °C to room temperature at 1 °C/min in the presence of a 6 T magnetic field. As expected, given the large separation between T_{ODT} and T_I, the neat materials did not show evidence of field-induced alignment of the hexagonally packed PLA cylinders. By contrast, highly aligned materials were produced when samples blended with the free mesogen were cooled from 85 °C in the presence of the field, as shown in Figure 5. From the 2D

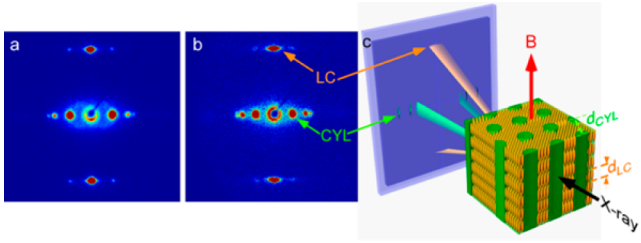

Figure 5. 2D SAXS patterns of highly oriented (a) LC12PLA2k and (b) LC12PLA2k-2 (R = 1) after magnetic field alignment. (c) The field is applied vertical as indicated. PLA cylinders (green) and the LC smectic layer normal are aligned along the applied field direction as depicted in the schematic.

scattering data it is apparent that the PLA cylinders are aligned parallel to the magnetic field direction and parallel to the smectic layer normal. This is consistent with the positive diamagnetic anisotropy and the expected planar anchoring of the CB mesogen at the PLA block interface (Figure S9, Supporting Information). We calculate an orientation order parameter, P_2, using the azimuthal distribution of the scattered intensity for the primary Bragg reflections of the BCP and LC mesophases as shown in equation S1 (Supporting Information). We obtain $P_2^{BCP} \sim 0.98$ and $P_2^{LC} \sim 0.99$ where 0 and 1 correspond to perfectly random and perfectly aligned systems, respectively. The data demonstrate that the magnetic field is extremely effective at aligning these materials.

Samples were similarly aligned containing a small amount (10 wt %) of a tetrafunctional thiol, pentaerythritol tetrakis(3-mercaptopropionate) cross-linker. Exposure to UV light for 30 min after alignment was effective in producing a mechanically robust cross-linked film as confirmed by insoluble film in tetrahydrofuran solvent. Subsequent mild basic hydrolysis of the samples in 0.5 M NaOH in (60/40) H_2O/MeOH was successful in selectively removing PLA chains as expected based on the control experiments performed on the neat LCBBC (Figure S10, Supporting Information).

Compared to other efforts to generate aligned nanoporous BCP-based materials,[11] the current approach differs in its explicit use of an external magnetic field to control the equilibrium morphology of the system over lateral and thickness dimensions that are not constrained by the physics of the process and in arbitrary directions that are not constrained by the geometry of the sample. This is significant as it provides a scalability aspect which is perhaps lacking in electric-field-driven alignment and removes the tenuous kinetic control and thickness limitations associated with solvent vapor based approaches. Further, the very high degree of alignment achieved using these materials is noteworthy given the general difficulty in approaching such high orientational order parameters using other methods or with other materials. Thus, this combination of magnetic field processing and the novel tailored materials introduced here represent a platform that provides a significant advance relative to currently utilized materials and methods.

In conclusion, we have demonstrated the design, synthesis, and optimization of a brush-type liquid crystalline block copolymer. The system demonstrates the key characteristics required for magnetic-field-directed self-assembly and the subsequent cross-linking and etch removal of the minority component to form nanoporous polymer films. The combination of structural control by molecular level design and scalable directed self-assembly offers a versatile platform for the development of selective transport media and functional materials using large-area, well-ordered nanoporous films as templates.

■ ASSOCIATED CONTENT

Supporting Information

Experimental procedures and additional figures/tables. This material is available free of charge via the Internet at http://pubs.acs.org.

■ AUTHOR INFORMATION

Corresponding Author

*E-mail: kasi@ims.uconn.edu.

Present Address

⊥CNMS, ORNL, Oak Ridge, TN 37831.

Author Contributions

#P.D. and M.G. contributed equally.

Notes

The authors declare no competing financial interest.

■ ACKNOWLEDGMENTS

This work was supported by NSF under CMMI-1246804. The authors would like to thank Mike Degen (Rigaku Inc.) and AMI Inc. for technical support. C.O. acknowledges additional financial support from NSF (DMR-0847534; DMR-1119826) and from 3M Nontenured Faculty Award. R.M.K. acknowledges additional financial support from NSF (DMR 0748398). Facilities use was supported by YINQE and NSF MRSEC DMR-1119826.

■ REFERENCES

(1) Hamley, I. W. *Nanotechnology* **2003**, *14*, R39−R54.
(2) Park, C.; Yoon, J.; Thomas, E. L. *Polymer* **2003**, *44*, 7779.
(3) Thurn-Albrecht, T.; Steiner, R.; DeRouchey, J.; Stafford, C. M.; Huang, E.; Bal, M.; Tuominen, M.; Hawker, C. J.; Russell, T. P. *Adv. Mater.* **2000**, *12*, 787.
(4) Rzayev, J.; Hillmyer, M. A. *J. Am. Chem. Soc.* **2005**, *127*, 13373.
(5) Phillip, W. A.; O'Neill, B.; Rodwogin, M.; Hillmyer, M. A.; Cussler, E. L. *ACS Appl. Mater. Interfaces* **2010**, *2*, 847.
(6) Peinemann, K.-V.; Abetz, V.; Simon, P. F. W. *Nat. Mater.* **2007**, *6*, 992.
(7) Yang, S. Y.; Ryu, I.; Kim, H. Y.; Kim, J. K.; Jang, S. K.; Russell, T. P. *Adv. Mater.* **2006**, *18*, 709.
(8) Jeong, U.; Ryu, D. Y.; Kho, D. H.; Kim, J. K.; Goldbach, J. T.; Kim, D. H.; Russell, T. P. *Adv. Mater.* **2004**, *16*, 533.
(9) Sidorenko, A.; Tokarev, I.; Minko, S.; Stamm, M. *J. Am. Chem. Soc.* **2003**, *125*, 12211.
(10) Mansky, P.; Liu, Y.; Huang, E.; Russell, T. P.; Hawker, C. *Science* **1997**, *275*, 1458.

(11) Darling, S. B. *Prog. Polym. Sci.* **2007**, *32*, 1152.
(12) Majewski, P. W.; Gopinadhan, M.; Osuji, C. O. *J. Polym. Sci., Part B: Polym. Phys.* **2012**, *50*, 2.
(13) Osuji, C.; Ferreira, P. J.; Mao, G.; Ober, C. K.; Vander Sande, J. B.; Thomas, E. L. *Macromolecules* **2004**, *37*, 9903.
(14) Gopinadhan, M.; Majewski, P. W.; Choo, Y.; Osuji, C. O. *Phys. Rev. Lett.* **2013**, *110*, 078301.
(15) Xia, Y.; Olsen, B. D.; Kornfield, J. A.; Grubbs, R. H. *J. Am. Chem. Soc.* **2009**, *131*, 18525.
(16) Rzayev, J. *ACS Macro Lett.* **2012**, *1*, 1146.
(17) Cavicchi, K. A.; Zalusky, A. S.; Hillmyer, M. A.; Lodge, T. P. *Macromol. Rapid Commun.* **2004**, *25*, 704.
(18) Hillmyer, M. A. In *Block Copolymers II*; Springer: New York, 2005; p 137.
(19) Chen, L.; Hillmyer, M. A. *Macromolecules* **2009**, *42*, 4237.
(20) Jackson, E. A.; Hillmyer, M. A. *ACS Nano* **2010**, *4*, 3548.
(21) Thurn-Albrecht, T.; Schotter, J.; Kästle, G. A.; Emley, N.; Shibauchi, T.; Krusin-Elbaum, L.; Guarini, K.; Black, C. T.; Tuominen, M. T.; Russell, T. P. *Science* **2000**, *290*, 2126.
(22) Mansky, P.; Harrison, C. K.; Chaikin, P. M.; Register, R. A.; Yao, N. *Appl. Phys. Lett.* **1996**, *68*, 2586.
(23) Mao, H.; Hillmyer, M. A. *Macromolecules* **2005**, *38*, 4038.
(24) Zalusky, A. S.; Olayo-Valles, R.; Taylor, C. J.; Hillmyer, M. A. *J. Am. Chem. Soc.* **2001**, *123*, 1519.
(25) Ryu, J.-H.; Park, S.; Kim, B.; Klaikherd, A.; Russell, T. P.; Thayumanavan, S. *J. Am. Chem. Soc.* **2009**, *131*, 9870.
(26) Gopinadhan, M.; Majewski, P. W.; Osuji, C. O. *Macromolecules* **2010**, *43*, 3286.
(27) Majewski, P. W.; Gopinadhan, M.; Jang, W.-S.; Lutkenhaus, J. L.; Osuji, C. O. *J. Am. Chem. Soc.* **2010**, *132*, 17516.
(28) Campos, L. M.; Killops, K. L.; Sakai, R.; Paulusse, J. M.; Damiron, D.; Drockenmuller, E.; Messmore, B. W.; Hawker, C. J. *Macromolecules* **2008**, *41*, 7063.
(29) Craig, A. A.; Imrie, C. T. *Macromolecules* **1995**, *28*, 3617.
(30) Osuji, C.; Chen, J.; Mao, G.; Ober, C.; Thomas, E. *Polymer* **2000**, *41*, 8897.
(31) Trimmel, G.; Riegler, S.; Fuchs, G.; Slugovc, C.; Stelzer, F. *Adv. Polym. Sci.* **2005**, *176*, 43.
(32) Gu, W.; Huh, J.; Hong, S. W.; Sveinbjornsson, B. R.; Park, C.; Grubbs, R. H.; Russell, T. P. *ACS Nano* **2013**, *7*, 2551.